

Matter Maps to Geometry in Gravitational Collapse

H. Khodabakhshi¹, Zhi-Chao Li¹, H. Lü^{1,2}, F. Shojai³

¹*Center for Joint Quantum Studies and Department of Physics,
School of Science, Tianjin University, Tianjin 300350, China*

²*The International Joint Institute of Tianjin University, Fuzhou,
Tianjin University, Tianjin 300350, China*

³*Department of Physics, University of Tehran, P.O. Box 14395-547, Tehran, Iran*

ABSTRACT

We establish an exact bidirectional map between interior Friedmann density of a collapsing star and exterior static spherically symmetric metric in generalized Oppenheimer–Snyder collapse. This reduces Einstein’s differential matter–geometry relation to an algebraic form, generating classical or quantum-corrected metrics and dynamics without solving field equations. Correction powers diagnose models: integer exponents signal ultraviolet completions, while fractional powers identify phenomenological ones. Our framework enables systematic tests of singularity resolution and cosmic censorship.

Contents

1	Introduction	2
2	Mapping collapse dynamics to static geometries	4
2.1	From density to geometry	5
2.2	From geometry to density	6
3	Integer-order corrections as a diagnostic of systematic UV-motivated expansions	7
4	Geometric classification of collapse dynamics	8
5	Conclusions and outlook	9
A	Classical realization of quantum-corrected geometry via nonlinear electrodynamics	10
B	Quantum-corrected Oppenheimer–Snyder collapse dynamics	12
C	Geometric classification and dynamical consistency	15

1 Introduction

Gravitational collapse need not end in a singularity. In the context of Oppenheimer–Snyder collapse [1] and its generalization to arbitrary static exteriors [2], an exact bidirectional mapping between interior matter content and exterior geometry provides a direct framework for generating black hole solutions and determining their collapse dynamics. By inserting physically motivated corrections into the total density ρ in the Friedmann equation, one can reconstruct the corresponding geometry and surface evolution.

While our prior work [2–4] established the generalized Oppenheimer–Snyder (GOS) framework, classified collapse outcomes into singular/bouncing/soft-landing scenarios, and conjectured an upper bound on horizon formation time (saturated by Schwarzschild), the present Letter introduces three new elements: (i) an exact bidirectional algebraic mapping that generates solutions without solving differential equations, (ii) a diagnostic criterion based on the analytic structure of density corrections to distinguish systematic UV-motivated expansions from phenomenological models, and (iii) an explicit construction demonstrating that loop quantum gravity (LQG)-corrected black hole geometries admit exact classical realizations in

nonlinear electrodynamics with identical collapse dynamics (see Appendices A–C for detailed derivations).

This mapping arises naturally from the GOS framework [2]. The force-free Israel junction conditions [5] restrict the exterior to the special class of static, spherically symmetric exterior metrics with $g_{tt}g_{rr} = -1$ [3], leading to the star’s surface evolution equation

$$\dot{R}^2 = 1 - f(R), \quad (1)$$

where the dot denotes differentiation with respect to the proper time T , the collapsing branch corresponds to $\dot{R} < 0$, and real motion requires $1 - f(R) \geq 0$. The interior homogeneous effective fluid satisfies an effective Friedmann equation $H^2 = 8\pi\rho/3$ with $H = \dot{R}/R$, where $\rho(R)$ is the star’s total effective density including standard matter together with all corrections from quantum effects, higher-derivative terms, or other physics. Combining these yields

$$\rho(R) = \frac{3}{8\pi R^2} [1 - f(R)], \quad (2)$$

where $\rho(R)$ decomposes into standard contributions ρ_s (neutral dust, radiation, and dark energy) and effective corrections ρ_{eff} from quantum or modified gravity effects. The relation is fully bidirectional: prescribing $\rho(R)$ reconstructs the exterior geometry $f(R)$, while any static solution $f(R)$ determines the effective density sourcing the collapse. Equation (2) thereby reduces the differential matter–geometry relation of Einstein’s field equations to a much simpler purely algebraic correspondence. Detailed derivations, explicit examples, and consistency analyses supporting all results are provided in Appendices A–C. Recent Hamiltonian-based work has shown that a one-parameter family of static, spherically symmetric metrics can be embedded into a class of generally covariant pure-gravity theories, thereby reconstructing the corresponding vacuum dynamics from geometry [12]. Within the GOS matching formalism, we do not attempt to reconstruct the covariant Hamiltonian theory for a given exterior metric. Instead, we establish a direct, bidirectional link between interior matter content and the exterior metric function $f(R)$.

Our mapping extends beyond Einstein–Maxwell theory. By inserting physically motivated corrections to the effective density ρ_{eff} —such as those from loop quantum cosmology (LQC) [6] or quasi-topological gravity [7]—one immediately obtains the corresponding black hole geometry. The structure of $\rho_{\text{eff}}(R)$ also helps diagnose whether a geometry is associated with a systematic UV-motivated expansion or is more naturally phenomenological. When corrections admit a Taylor expansion in integer powers of ρ_m —as in systematic UV-motivated perturbative expansions such as LQG or quasi-topological gravity—the resulting metric function $f(R)$ contains only terms of the form $R^{-(3n-2)}$ with $n \in \mathbb{N}$. In contrast, phenomenological models like

the Bardeen black hole [8] typically involve non-analytic or fractional powers of R , indicating an effective rather than fundamental origin.

In Ref. [4], we showed that the shape of $f(R)$ determines whether collapse ends in a singularity, bounces at finite radius, or approaches the center only asymptotically—leading to the three scenarios: *singular*, *bouncing*, and *soft-landing*. Here, we use this classification as a diagnostic for the mapping (2). In Appendix A, we construct... an exact nonlinear electrodynamics (NLED) counterpart of an LQG-corrected black hole [9,10]. With matched parameters, both yield identical $R(T)$ and apparent-horizon evolutions. Similarly, the Hayward metric [11] exhibits soft-landing collapse with a de Sitter core, while its large- R expansion shares the same leading correction as the LQG-inspired metric, illustrating that identical leading asymptotic corrections need not imply identical global collapse dynamics. We work in units $G = c = 1$ and metric signature $(-, +, +, +)$.

2 Mapping collapse dynamics to static geometries

In the GOS framework, force-free matching requires continuity of radial stress across the star's surface Σ . Interpreting the exterior metric as sourced by an anisotropic fluid with $T^\mu{}_\nu = \text{diag}(-\rho_{\text{out}}, p_r, p_t, p_t)$, the exterior energy density and pressures are [2]

$$\rho_{\text{out}}(R) = -p_{r,\text{out}}(R) = \frac{1 - f(R) - Rf'(R)}{8\pi R^2}, \quad (3)$$

$$p_{t,\text{out}}(R) = \frac{1}{8\pi} \left(\frac{f'(R)}{R} + \frac{f''(R)}{2} \right). \quad (4)$$

The interior effective pressure follows from energy conservation $\dot{\rho} + 3H(\rho + p_{\text{in}}) = 0$, yielding

$$p_{\text{in}}(R) = -\frac{\dot{\rho}}{3H} - \rho = p_{r,\text{out}}(R), \quad (5)$$

where we used the mapping (2) and the surface equation (1). Thus, the mapping automatically ensures force-free matching: no thin shell is required, and the junction is smooth by construction.

The effective density decomposes naturally as

$$\rho(R) = \rho_s(R) + \rho_{\text{eff}}(R), \quad \rho_s(R) = \frac{3}{4\pi} \left(\frac{\alpha}{R^3} + \frac{\beta}{R^4} + \gamma\Lambda \right), \quad (6)$$

where ρ_s contains standard contributions (neutral dust, electromagnetic field energy, and dark energy) and ρ_{eff} encodes corrections from quantum or modified gravity effects. The R^{-3} term corresponds to neutral dust density $\rho_m = 3M/(4\pi R^3)$. The R^{-4} term originates from the electromagnetic field energy density produced by a charge concentrated in the core [4]; although it shares the same radial scaling as radiation, it represents stored field energy rather than

actual radiation or charged matter. This identification is evaluated strictly at the surface Σ , where the force-free Israel junction conditions depend only on the local metric and energy density. Detailed electromagnetic dynamics in the deep interior do not affect the matching. Furthermore, as shown in the geometric classification below, the surface always bounces at $R_* < R_-$ and never reaches the charged core, rendering the neutral-dust assumption at Σ dynamically self-consistent throughout the collapse. For $\rho_{\text{eff}} = 0$, substituting (6) into (2) reproduces the Reissner–Nordström (RN)–(A)dS metric

$$f_{\text{RN}}(R) = 1 - \frac{2M}{R} + \frac{q^2}{R^2} - \frac{\Lambda}{3}R^2, \quad (7)$$

with coefficients fixed by matching:

$$\alpha = M, \quad \beta = -\frac{q^2}{2}, \quad \gamma = \frac{1}{6}. \quad (8)$$

Setting $\beta = \gamma = 0$ recovers the Schwarzschild solution.

The mapping (2) operates bidirectionally: (i) prescribing $\rho(R)$ reconstructs $f(R)$ algebraically; (ii) given $f(R)$, one extracts the effective density sourcing the collapse. Its power becomes evident when incorporating corrections.

2.1 From density to geometry

LQC replaces the classical density with the Ashtekar–Pawlowski–Singh (APS) form [6]

$$\rho_{\text{APS}}(R) = \rho_{\text{m}} \left(1 - \frac{\rho_{\text{m}}}{\rho_{\text{c}}} \right), \quad \rho_{\text{m}} = \frac{3M}{4\pi R^3}, \quad (9)$$

where the second term encodes quantum corrections. Substituting (9) into (2) yields the quantum-corrected Schwarzschild metric [9]

$$f_{\text{q-Sch}}(R) = 1 - \frac{2M}{R} + \frac{4\ell^2 M^2}{R^4}, \quad \ell^2 = \frac{3}{8\pi\rho_{\text{c}}}, \quad (10)$$

with $\ell^2 = \gamma^2 \Delta$ setting the short-distance scale (γ : Barbero–Immirzi parameter; Δ : area gap). Charged and cosmological extensions follow immediately via the universal substitution $\rho_{\text{m}} \rightarrow \rho_{\text{s}}$ in (9):

$$f_{\text{q-RN}}(R) = f_{\text{RN}}(R) + \frac{\ell^2}{R^2} [1 - f_{\text{RN}}(R)]^2. \quad (11)$$

This algebraic extension reconstructs the geometry directly from the density ansatz, avoiding the need to solve the full set of modified differential field equations.

2.2 From geometry to density

Starting from a known $f(R)$ reveals the physical content of regular black holes. Quantum-corrected geometries can also arise from classical NLED, which introduces an extra degree of freedom. The LQG-corrected Schwarzschild metric (10) is reproduced by the NLED Lagrangian [10]

$$\mathcal{L}(F) = -\frac{\eta}{16\pi}F^{3/2}, \quad \eta > 0, \quad (12)$$

with purely magnetic field $F_{\theta\phi} = Q_m \sin\theta$. The energy density is $\rho(R) = \eta\sqrt{2}Q_m^3/(8\pi R^6)$. Integrating $m'(R) = 4\pi R^2\rho(R)$ gives

$$f(R) = 1 - \frac{2M}{R} + \frac{\eta\sqrt{2}Q_m^3}{3R^4}, \quad (13)$$

Matching to (10) requires $\eta\sqrt{2}Q_m^3/3 = 4\ell^2 M^2$, or $Q_m = (12\ell^2/(\eta\sqrt{2}))^{1/3}M^{2/3}$, relating the magnetic charge Q_m to the quantum scale ℓ^2 (see Appendix A). Thus identical geometries can emerge from distinct physical origins.

The Hayward metric [11]

$$f_{\text{Hay}}(R) = 1 - \frac{2M/R}{1 + 2M\tilde{\ell}^2/R^3} \quad (14)$$

maps to the effective density

$$\rho_{\text{Hay}}(R) = \rho_m \left(1 + \frac{\rho_m}{\tilde{\rho}_c}\right)^{-1}, \quad \tilde{\ell}^2 = \frac{3}{8\pi\tilde{\rho}_c}. \quad (15)$$

In the limit $\tilde{\ell}^2 \ll 1$, this agrees with the APS form (9) at leading order, showing that Hayward gravity and LQG corrections share the same leading-order behavior. Applying $\rho_m \rightarrow \rho_s$ to (15) yields the charged Hayward–(A)dS solution

$$f_{\text{Hay-ch}}(R) = 1 - [1 - f_{\text{RN}}(R)] \left(1 + \frac{\tilde{\ell}^2}{R^2}[1 - f_{\text{RN}}(R)]\right)^{-1}, \quad (16)$$

which agrees at leading order with (11) when $\tilde{\ell}^2 \ll 1$.

The Bardeen metric [8]

$$f_{\text{Bar}}(R) = 1 - \frac{2M}{R} \left(1 + \frac{g^2}{R^2}\right)^{-3/2} \quad (17)$$

corresponds to

$$\rho_{\text{Bar}}(R) = \rho_m \left[1 + \left(\frac{\rho_m}{\tilde{\rho}_c}\right)^{2/3}\right]^{-3/2}, \quad g^2 = \left(\frac{3M}{4\pi\tilde{\rho}_c}\right)^{2/3}. \quad (18)$$

Expanding for small $g^2 \ll 1$ gives

$$\rho_{\text{Bar}}(R) = \rho_{\text{m}} \left(1 - \frac{3}{2} \left(\frac{\rho_{\text{m}}}{\rho_{\text{c}}} \right)^{2/3} + \dots \right), \quad (19)$$

which involves fractional powers of ρ_{m} . Unlike the APS and Hayward densities—which admit Taylor expansions in integer powers of $\rho_{\text{m}}/\rho_{\text{c}}$ —the Bardeen density contains fractional, non-integer powers. This indicates that the Bardeen solution originates from a phenomenological model. Nevertheless, the mapping applies universally: substituting $\rho_{\text{m}} \rightarrow \rho_{\text{s}}$ in (18) yields the charged Bardeen-(A)dS solution without solving field equations.

In summary, the mapping (2) provides a unified algebraic framework for generating black hole solutions and predicting their collapse dynamics across classical and quantum theories.

3 Integer-order corrections as a diagnostic of systematic UV-motivated expansions

The structure of density corrections can diagnose whether a metric is compatible with a systematic UV-motivated expansion or is more naturally interpreted phenomenologically. Writing the total effective density as

$$\rho(R) = \rho_{\text{m}} \mathcal{F} \left(\frac{\rho_{\text{m}}}{\rho_{\text{c}}} \right), \quad (20)$$

a correction is of *integer order* precisely when \mathcal{F} admits a Taylor expansion in integer powers of the dimensionless ratio $x = \rho_{\text{m}}/\rho_{\text{c}}$:

$$\mathcal{F}(x) = 1 + c_1 x + c_2 x^2 + c_3 x^3 + \dots. \quad (21)$$

Within the ansatz (20), this pattern is equivalent to requiring that the metric function contains exclusively terms of the form $R^{-(3n-2)}$ in $1 - f(R)$:

$$1 - f(R) = \frac{2M}{R} + \frac{a_2 M^2}{R^4} + \frac{a_3 M^3}{R^7} + \frac{a_4 M^4}{R^{10}} + \dots. \quad (22)$$

We emphasize that this diagnostic identifies theories with a *systematic perturbative expansion* in a dimensionless coupling; non-analytic terms may arise from non-perturbative effects, and integer-order expansions can appear in effective theories. The criterion is most powerful when combined with independent theoretical constraints. Each power $R^{-(3n-2)}$ maps directly to a density correction proportional to ρ_{m}^n , reflecting a systematic expansion in a dimensionless coupling. This integer-order pattern is preserved under the universal substitution $\rho_{\text{m}} \rightarrow \rho_{\text{s}}$, where $\rho_{\text{s}} = 3M/(4\pi R^3) - 3q^2/(8\pi R^4) + \Lambda/(8\pi)$ incorporates dust, charge, and cosmological constant contributions. The diagnostic thus applies to charged and asymptotically (A)dS

extensions as an expansion in ρ_s ; the simple inverse-radius test $R^{-(3n-2)}$ should be understood as the neutral limit.

LQG provides the prototype: the Ashtekar–Pawlowski–Singh density yields the quantum-corrected Schwarzschild metric with only the R^{-4} term at leading order. Higher holonomy corrections generate R^{-7} , R^{-10} , and so on, preserving the integer structure throughout. Applying $\rho_m \rightarrow \rho_s$ extends this directly to the quantum-corrected RN–(A)dS solution (11), which retains the same pattern. Similarly, generalized quasi-topological gravity (e.g., Einsteinian cubic gravity [13]) and regularized Einstein–Gauss–Bonnet gravity [14] produce metrics of the form (22); their charged/(A)dS extensions inherit the same structure. The Hayward metric also follows this pattern: its expansion contains only $R^{-(3n-2)}$ terms, and for small $\tilde{\ell}^2$ it agrees at leading order with the LQG correction.

In contrast, the Bardeen black hole introduces R^{-3} and R^{-5} terms in $1 - f(R)$, violating (22). This yields fractional powers in the density expansion—specifically $(\rho_m/\bar{\rho}_c)^{2/3}$ —signaling a phenomenological origin. Even after extending to charged solutions via $\rho_m \rightarrow \rho_s$, the fractional powers persist in charged/(A)dS extensions, supporting its interpretation as an effective phenomenological model rather than as a simple perturbative UV expansion. Within this diagnostic, any metric failing to satisfy this integer-order structure is best regarded as an effective or phenomenological model rather than as the low-energy expansion of a systematic UV-motivated expansion.

This diagnostic is independent of the collapse outcome. Both integer-order and fractional corrections can produce bouncing or soft-landing collapse, depending solely on $f(R)$. Our mapping therefore provides a simple criterion: given any static solution $f(R)$, expand $1 - f(R)$ in inverse powers of R . If every term follows $R^{-(3n-2)}$, the solution is compatible with a systematic UV-motivated expansion; otherwise, it is more naturally interpreted as phenomenological. Conversely, the presence of fractional powers does not automatically invalidate a model; it suggests that the ansatz may be phenomenological or that the expansion parameter is not simply ρ_m/ρ_c . Such models can still provide valuable effective descriptions of high-curvature physics.

4 Geometric classification of collapse dynamics

The collapse dynamics are entirely governed by the exterior metric function $f(R)$ in Eq. (1) through $1 - f(R) \geq 0$. This leads to three possible outcomes [4]: *singular* collapse, where the surface reaches $R = 0$ in finite proper time; *bouncing* collapse, where $f(R_*) = 1$ and $f'(R_*) < 0$ at finite $R_* > 0$; and *soft-landing* collapse, where $f(R) < 1$ for all $R > 0$ but

$f(R) \rightarrow 1$ as $R \rightarrow 0$ (with true curvature regularity requiring a de Sitter-like core [15]). In the bouncing case, consistency of the trapped region requires $R_* < R_-$ and, more strictly, the apparent-horizon minimum to lie inside the inner horizon.

Moreover, physical consistency imposes strict hierarchies between the apparent-horizon minimum and the event horizons. For example, in RN-like collapse, requiring the minimum to lie inside the inner horizon yields parameter bounds analogous to Eq. (30) in Ref. [4]. The collapse class is determined not by the functional *form* of $f(R)$, but by its *parameter values*. The Hayward metric (14), for example, realizes bouncing behavior for $\tilde{\ell}^2 \ll M^2$ but transitions to soft-landing as $\tilde{\ell}^2$ increases (see Appendix C). More generally, distinct physical origins can produce identical collapse dynamics when $f(R)$ coincides. The LQG-corrected metric admits an exact classical counterpart in Einstein gravity coupled to NLED [10] under the parameter matching $\eta\sqrt{2}Q_m^3/3 = 4\ell^2M^2$. When satisfied, quantum and classical descriptions yield indistinguishable surface trajectories, apparent-horizon evolution, and horizon structure.

Both descriptions respect cosmic censorship. After bouncing at $R_* < R_-$, the surface moves outward toward the inner horizon R_- . Generic perturbations near R_- trigger mass inflation [17], producing a weak null singularity that replaces the Cauchy horizon. The classical $R = 0$ singularity remains causally disconnected, preserving weak cosmic censorship [18]. The mass-inflation singularity at R_- upholds strong cosmic censorship [19]. Thus, the physically relevant endpoint occurs near R_- , not at the center (see Appendix C for detailed analysis).

5 Conclusions and outlook

We have established an exact bidirectional mapping between the interior matter content of a collapsing star and the exterior black hole geometry within the GOS framework. Inserting physically motivated corrections into the effective density of the Friedmann equation directly yields the complete black hole geometry and its collapse dynamics. This approach works uniformly across LQG, quasi-topological gravity, nonlinear electrodynamics, and regular black hole models.

Two points emerge clearly. First, the fate of collapse—singular, bouncing, or soft-landing—is fixed by the exterior metric function $f(R)$. This is illustrated by the equivalence between LQG corrections and classical nonlinear electrodynamics: with matched parameters, the resulting surface trajectories and horizon evolution are the same. Second, the mathematical structure of density corrections distinguishes systematic UV-motivated perturbative expansions from more phenomenological models. Integer-order expansions in ρ_m/ρ_c —producing metric terms $R^{-(3n-2)}$ —are characteristic of the former, while fractional powers, as in the

Bardeen black hole, indicate the latter. Within the GOS matching framework, Eq. (2) reduces the differential matter–geometry relation of Einstein’s field equations to a much simpler purely algebraic correspondence.

Finally, we remark that our algebraic mapping complements Hamiltonian-based reconstruction methods [12]. There, covariant vacuum theories are reconstructed from a prescribed family of static, spherically symmetric metrics; here, within the GOS matching framework, the exterior geometry and collapse dynamics are reconstructed algebraically from interior effective density corrections, and conversely the effective density is extracted from any chosen exterior metric. The two approaches thus address distinct layers of the same broader question: the covariant dynamics underlying a vacuum geometry versus the matter content driving a dynamical collapse.

Future work will extend this framework to rotating collapse and inhomogeneous interiors, where angular momentum and density gradients may reveal new dynamical regimes. The integer-order diagnostic can guide the construction of systematic quantum corrections in string-motivated higher-derivative theories. Observational signatures—gravitational wave echoes from bouncing collapse, shadow deformations in soft-landing scenarios, or imprints on ringdown spectra—can now be systematically explored using geometries generated algebraically.

Acknowledgement

This work is supported in part by the National Natural Science Foundation of China (NSFC) Grant Nos. W2533015, 12375052, and 11935009 and by the Tianjin University Self-Innovation Fund for Extreme Basic Research Grant No. 2025XJ21-0007.

Appendix

A Classical realization of quantum-corrected geometry via non-linear electrodynamics

We emphasize that NLED serves here as a classical completion engineered to reproduce a prescribed $f(R)$, with the magnetic charge providing an additional degree of freedom. It is not intended as a fundamental electromagnetic theory with a Maxwell weak-field limit. Consider the action

$$S = \int d^4x \sqrt{-g} \left[\frac{\mathcal{R}}{16\pi} + \mathcal{L}(F) \right], \quad (23)$$

where $F = F_{\mu\nu}F^{\mu\nu}$ and \mathcal{R} is the Ricci scalar. The stress tensor and generalized Maxwell equation read

$$T_{\mu\nu} = -4\mathcal{L}_F F_{\mu\alpha}F_{\nu}^{\alpha} + g_{\mu\nu}\mathcal{L}, \quad \nabla_{\mu}(\mathcal{L}_F F^{\mu\nu}) = 0, \quad (24)$$

where $\mathcal{L}_F \equiv d\mathcal{L}/dF$. We adopt a purely magnetic, spherically symmetric configuration $F_{\theta\phi} = Q_m \sin\theta$, which respects spherical symmetry and describes a conserved magnetic charge. For this configuration the invariant is $F = 2Q_m^2/R^4 > 0$. Purely magnetic fields satisfy $T^t_t = T^R_R = \mathcal{L}$ and $T^\theta_\theta = T^\phi_\phi = \mathcal{L} - 2F\mathcal{L}_F$, giving

$$\rho = -\mathcal{L}, \quad p_r = -\rho, \quad p_t = \mathcal{L} - 2F\mathcal{L}_F. \quad (25)$$

Since $F \propto R^{-4}$ for a magnetic monopole, choosing $\mathcal{L} \propto -F^{3/2}$ yields

$$\mathcal{L}(F) = -\frac{\eta}{16\pi} F^{3/2}, \quad \eta > 0, \quad (26)$$

giving the energy density and pressures

$$\rho(R) = -p_r(R) = \frac{p_t(R)}{2} = \frac{\eta\sqrt{2}Q_m^3}{8\pi R^6}, \quad (27)$$

where we take $Q_m > 0$ without loss of generality. The weak and strong energy conditions are satisfied everywhere, while the dominant energy condition is violated ($p_t = 2\rho > \rho$). However, because $\rho \propto R^{-6}$ decays rapidly, this violation is confined to the high-curvature core and has negligible macroscopic impact. Such localized dominant-energy-condition violation is a known feature of many regular black-hole models sourced by nonlinear electrodynamics [10,21]. Since the violation is confined to the high-curvature core ($R \ll M$) and the weak/strong energy conditions hold everywhere, the macroscopic dynamics and junction conditions remain physically consistent. Moreover, because the bounce occurs at $R_* < R_-$ while remaining outside the charged core region, the effective description at the matching surface Σ is insensitive to the detailed high-curvature behavior.

Writing the metric function as $f(R) = 1 - 2m(R)/R$, Einstein's equations yield the Misner–Sharp mass relation $m'(R) = 4\pi R^2 \rho(R)$ [20]. Substituting Eq. (27) gives $m'(R) = \eta\sqrt{2}Q_m^3/(2R^4)$, which integrates to

$$m(R) = M - \frac{\eta\sqrt{2}Q_m^3}{6R^3}, \quad f(R) = 1 - \frac{2M}{R} + \frac{\eta\sqrt{2}Q_m^3}{3R^4}. \quad (28)$$

Matching to the quantum-corrected form (10) requires

$$\frac{\eta\sqrt{2}Q_m^3}{3} = 4\ell^2 M^2, \quad \text{or} \quad Q_m = \left(\frac{12\ell^2}{\eta\sqrt{2}}\right)^{1/3} M^{2/3}. \quad (29)$$

Thus the magnetic charge scales as $Q_m \propto M^{2/3}$, requiring mass-dependent tuning to reproduce the same exterior geometry.

The identical spacetime therefore admits two distinct interpretations. In the quantum picture, short-distance repulsion comes from LQG corrections encoded in ℓ^2 . In the classical picture, the same geometry emerges as an exact solution of Einstein gravity coupled to NLED, where a magnetic monopole provides the repulsive core. The additional degree of freedom Q_m can be tuned to reproduce precisely the R^{-4} correction of the quantum-corrected metric, yielding identical exterior geometry without including quantum effects.

B Quantum-corrected Oppenheimer–Snyder collapse dynamics

We model gravitational collapse as a homogeneous dust interior ($k = 0$ FRW) matched to a static spherically symmetric exterior under force-free Darmois–Israel junction conditions. The exterior metric reads

$$ds_{\text{out}}^2 = -f(R) dt^2 + \frac{dR^2}{f(R)} + R^2 d\Omega^2, \quad (30)$$

and the star’s surface at fixed comoving radius r_Σ has areal radius $R(\tau) = a(\tau)r_\Sigma$, where τ is the proper time of comoving interior observers. Working in Painlevé–Gullstrand coordinates, which are regular across horizons and synchronized with τ , the junction conditions yield the surface evolution law

$$\dot{R}^2 = 1 - f(R), \quad (31)$$

where the collapsing branch takes $\dot{R} < 0$. Real motion requires $1 - f(R) \geq 0$. In the absence of a thin shell, the junction conditions require continuity of radial stress across Σ , which is automatically satisfied by the mapping (2).

The surface trajectory follows from integrating Eq. (31):

$$T(R) = \int_R^{R_0} \frac{dR'}{\sqrt{1 - f(R')}}, \quad (32)$$

with R_0 the initial radius. The apparent horizon inside the star is

$$R_{\text{AH}}(R) = \frac{R}{\sqrt{1 - f(R)}}, \quad (33)$$

which diverges at a bounce where $f(R_*) = 1$. The interior event horizon, obtained by tracing outgoing null geodesics backward from the outer horizon R_+ (where $f(R_+) = 0$), is given by

$$R_{\text{eh}}(R) = R \left(1 - \int_{R_+}^R \frac{dR'}{R' \sqrt{1 - f(R')}} \right), \quad (34)$$

satisfying $R_{\text{eh}}(R_+) = R_+$ and $R_{\text{eh}}(R) < R$ for $R > R_+$.

Equations (31)–(34) demonstrate that the entire collapse dynamics and horizon structure depend only on the exterior metric function $f(R)$. This permits two equivalent approaches: (i) begin with an effective interior dynamics (e.g., LQC) and reconstruct $f(R)$, or (ii) specify a candidate exterior $f(R)$ and derive the induced surface evolution. When the Darmois–Israel conditions hold without a thin shell, both descriptions are dynamically equivalent on the surface Σ .

We now analyze the collapse dynamics for the quantum-corrected metric

$$f_{\text{qOS}}(R) = 1 - \frac{2M}{R} + \frac{\alpha M^2}{R^4}, \quad \alpha \equiv 4\ell^2, \quad (35)$$

which arises both from LQG corrections [9] and from the NLED realization (Appendix A) when $\alpha = \eta\sqrt{2}Q_m^3/(3M^2)$. This example concretely illustrates bouncing collapse without repeating analyses of RN or regular black holes from prior work [4].

Under force-free junction conditions, the star’s surface evolves via $\dot{R}^2 = 1 - f_{\text{qOS}}(R)$ with $\dot{R} < 0$ during collapse. Integrating yields the proper time to radius R :

$$T(R) = \frac{1}{3\sqrt{M}} \left[\sqrt{2R_0^3 - \alpha M} - \sqrt{2R^3 - \alpha M} \right], \quad (36)$$

where R_0 is the initial radius. The bounce occurs at $R_* = (\alpha M/2)^{1/3}$ where $\dot{R} = 0$ and $\ddot{R} > 0$, with bounce time $T_* = T(R_*)$.

Three characteristic radii govern the dynamics, forming the strict hierarchy $R_{\text{infl}} > R_{\text{turn}} > R_*$:

$$\begin{aligned} R_*^3 &= \frac{\alpha M}{2}, & (\dot{R} = 0, \text{ bounce}), \\ R_{\text{turn}}^3 &= \alpha M = 2R_*^3, & (dR_{\text{AH}}/dT = 0, \text{ apparent-horizon vertex}), \\ R_{\text{infl}}^3 &= 2\alpha M = 4R_*^3, & (\ddot{R} = 0, \text{ inflection point}). \end{aligned} \quad (37)$$

The surface accelerates for $R > R_{\text{infl}}$ and decelerates for $R_* < R < R_{\text{infl}}$. The apparent horizon radius is $R_{\text{AH}}(R) = R/\sqrt{1 - f_{\text{qOS}}(R)}$, which diverges at R_* .

Horizons satisfy $f_{\text{qOS}}(R) = 0$, i.e., $R^4 - 2MR^3 + \alpha M^2 = 0$. A degenerate case ($f = f' = 0$) occurs at $\alpha_{\text{crit}} = 27M^2/16$ with $R^{(\text{deg})} = 3M/2$. For $0 < \alpha < \alpha_{\text{crit}}$, two horizons exist; for $\alpha > \alpha_{\text{crit}}$, none. In the weak-correction regime $\alpha/M^2 \ll 1$,

$$R_- \simeq R_*, \quad R_+ \simeq 2M - \frac{\alpha}{8M}, \quad (38)$$

with $R_- > R_*$ holding exactly.

Physical consistency of the trapped region requires the apparent-horizon minimum to form inside the inner horizon: $R_{\text{turn}} < R_-$. Using $f_{\text{qOS}}(R_{\text{turn}}) = 1 - M/R_{\text{turn}}$, the boundary case

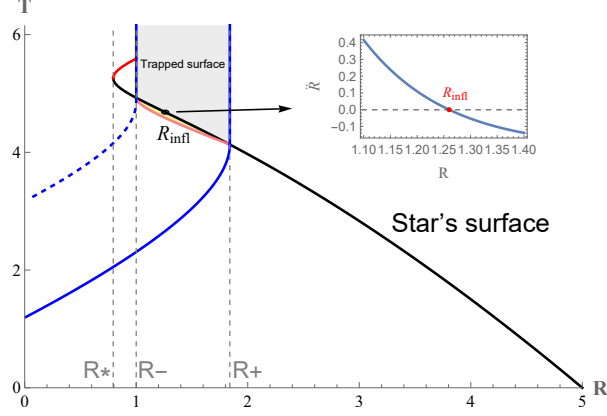


Figure 1: Surface trajectory $R(T)$ for gravitational collapse with $M = 1$ (in Planck units), initial radius $R_0 = 5$, and quantum correction parameter $\alpha = 1$. The star bounces at $R_* \simeq 0.79$ between the inner and outer horizons $R_- \simeq 1.00$ and $R_+ \simeq 1.84$. Inset: proper acceleration \ddot{R} changes sign at the inflection point $R_{\text{infl}} \simeq 1.26$, marking the transition from acceleration to deceleration.

$R_{\text{turn}} = R_-$ gives $R_{\text{turn}} = M$ and $\alpha = M^2$. Thus, consistent apparent-horizon minimum formation requires

$$\alpha < M^2 \quad (\text{in addition to } \alpha < \alpha_{\text{crit}}), \quad (39)$$

which translates via the NLED matching condition (29) into an upper bound on the magnetic charge Q_m .

Following the bounce, the surface evolves toward R_- where mass inflation [17] generically produces a weak null singularity. The classical $R = 0$ singularity remains causally disconnected, preserving weak cosmic censorship [18]. The mass-inflation singularity at R_- upholds strong cosmic censorship [19] by converting the Cauchy horizon into a curvature singularity. Hence, the physically relevant endpoint occurs near R_- .

This analysis confirms that the entire collapse dynamics—surface trajectory (32), apparent horizon (33), event horizon (34), characteristic radii, and cosmic censorship implications—depends solely on $f_{\text{QOS}}(R)$. Whether derived from quantum geometry or classical NLED, identical $f(R)$ yields identical physics. The mapping framework thus provides a geometric lens: singularity resolution is encoded in spacetime structure alone, independent of microscopic origin.

C Geometric classification and dynamical consistency

This section provides the rigorous derivations supporting the collapse classification discussed in the main text.

Hierarchy of characteristic radii. For bouncing collapse, the turning point R_* satisfies $f(R_*) = 1$ and $f'(R_*) < 0$. Physical motion requires $1 - f(R) \geq 0$, so the region $0 < R < R_*$ is classically forbidden and implies $f(R) > 1$. Suppose, for contradiction, that $R_* \geq R_-$, where R_- is the inner horizon satisfying $f(R_-) = 0$. Since R_- would then lie in the forbidden region, we would have $f(R_-) > 1$, directly contradicting the horizon definition. Hence $R_* < R_-$ strictly. This hierarchy holds for any static metric with two horizons and ensures the bounce occurs outside the charged core, preserving the neutral-dust assumption at the matching surface Σ [4]. For broader horizon-counting constraints under energy conditions, see Ref. [16].

Physical consistency of the trapped region further requires the apparent-horizon minimum to form inside the inner horizon: $R_{\text{turn}} < R_-$. Using the quantum-corrected metric (35), we have $f_{\text{qOS}}(R_{\text{turn}}) = 1 - M/R_{\text{turn}}$. Imposing the boundary case $R_{\text{turn}} = R_-$ yields $R_{\text{turn}} = M$ and $\alpha = M^2$. Thus, consistent apparent-horizon formation requires

$$\alpha < M^2 \quad (\text{in addition to } \alpha < \alpha_{\text{crit}}), \quad (40)$$

which translates via the NLED matching condition (29) into an upper bound on the magnetic charge Q_m . Numerical verification of this hierarchy is shown in Fig. 1 of Appendix B.

Hayward soft-landing and asymptotic expansion. Expanding the Hayward metric (14) yields

$$1 - f_{\text{Hay}}(R) = \frac{2M}{R} - \frac{4M^2\tilde{\ell}^2}{R^4} + \frac{8M^3\tilde{\ell}^4}{R^7} - \dots \quad (41)$$

This expansion reproduces the LQG-corrected form (10) only at leading order in the large- R expansion. It should not be interpreted as a finite-radius bounce of the full Hayward geometry. Indeed, for the full rational metric, $1 - f_{\text{Hay}}(R) = 2M/[R(1 + 2M\tilde{\ell}^2/R^3)] > 0$ for all $R > 0$, so $f_{\text{Hay}}(R) = 1$ has no positive finite-radius root. The Hayward metric therefore realizes soft-landing collapse, with $f_{\text{Hay}}(R) < 1$ for all $R > 0$ and $f_{\text{Hay}}(R) \rightarrow 1$ as $R \rightarrow 0$. Note that $f(0) = 1$ alone does not ensure curvature regularity; some higher-derivative models (e.g., Einstein–Gauss–Bonnet [4]) satisfy this condition yet retain a central singularity. True regularity demands a de Sitter-like core near $R = 0$ with $\rho + p_r = 0$ and $\rho + p_t > 0$, satisfying the weak and strong energy conditions [15].

Mass inflation and cosmic censorship. After bouncing at $R_* < R_-$, the surface evolves toward the inner horizon. Generic perturbations near R_- trigger mass inflation [17], producing a weak null singularity that replaces the Cauchy horizon. The classical $R = 0$ singularity remains causally disconnected, preserving weak cosmic censorship [18]. The mass-inflation singularity at R_- upholds strong cosmic censorship [19] by converting the Cauchy horizon into a curvature singularity. Hence the physically relevant dynamical endpoint occurs near R_- , not at the center. This mechanism applies universally to any $f(R)$ yielding bouncing dynamics.

References

- [1] J. R. Oppenheimer and H. Snyder, “On continued gravitational contraction,” *Phys. Rev.* **56**, 455–459 (1939). doi:10.1103/PhysRev.56.455
- [2] H. Khodabakhshi, H. Lü, and F. Shojai, “Gravitational collapse: generalizing Oppenheimer–Snyder and a conjecture on horizon formation time,” *Phys. Rev. D* **112**, 124057 (2025). doi:10.1103/PhysRevD.112.124057 arXiv:2506.03702 [gr-qc]
- [3] Z. C. Li, H. Khodabakhshi, and H. Lü, “The upper bound of event horizon formation time in generalized Oppenheimer–Snyder collapse,” *Phys. Lett. B* **861**, 140245 (2026). doi:10.1016/j.physletb.2026.140245 arXiv:2512.24421 [gr-qc]
- [4] Z. C. Li, H. Khodabakhshi, and H. Lü, “Classification of Oppenheimer–Snyder Collapse: Singular, Bouncing, and Soft-Landing Scenarios,” arXiv:2602.04956 [gr-qc] (2026).
- [5] W. Israel, “Singular hypersurfaces and thin shells in general relativity,” *Nuovo Cimento B* **44**, 1 (1966); [Erratum: *Nuovo Cimento B* **48**, 463 (1967)]. doi:10.1007/BF02710419
- [6] A. Ashtekar, T. Pawłowski, and P. Singh, “Quantum nature of the big bang: An analytical description,” *Phys. Rev. D* **73**, 124038 (2006). doi:10.1103/PhysRevD.73.124038 arXiv:gr-qc/0604013
- [7] P. Bueno, P. A. Cano, and R. A. Hennigar, “Regular black holes from pure gravity,” *Phys. Lett. B* **861**, 139260 (2025). doi:10.1016/j.physletb.2025.139260 arXiv:2403.04827 [gr-qc]
- [8] J. M. Bardeen, “Non-singular general relativistic gravitational collapse,” in *Proceedings of the International Conference GR5* (Tbilisi, Georgia, 9–16 September 1968), p. 174.
- [9] B. Kelly *et al.*, “Loop quantum gravity corrections to black hole interiors,” *Class. Quant. Grav.* **38**, 03LT01 (2021). doi:10.1088/1361-6382/abd43c arXiv:2006.09344 [gr-qc]

- [10] E. Ayón-Beato and A. García, “Regular black hole in general relativity coupled to nonlinear electrodynamics,” *Phys. Rev. Lett.* **80**, 5056–5059 (1998). doi:10.1103/PhysRevLett.80.5056 arXiv:gr-qc/9911046
- [11] S. A. Hayward, “Formation and evaporation of nonsingular black holes,” *Phys. Rev. Lett.* **96**, 031103 (2006). doi:10.1103/PhysRevLett.96.031103 arXiv:gr-qc/0506126
- [12] C. Zhang and Z. Cao, “Covariant dynamics from static spherically symmetric geometries,” *Phys. Rev. Lett.* **135**, 261401 (2025), arXiv:2506.09540 [gr-qc].
- [13] P. Bueno and P. A. Cano, “Einsteinian cubic gravity,” *Phys. Rev. D* **94**, 104005 (2016). doi:10.1103/PhysRevD.94.104005 arXiv:1607.06463 [hep-th]
- [14] D. Glavan and C. Lin, “Einstein-Gauss-Bonnet gravity in four-dimensional space-time,” *Phys. Rev. Lett.* **124**, 081301 (2020). doi:10.1103/PhysRevLett.124.081301 arXiv:1905.03601 [gr-qc]
- [15] Z. C. Li and H. Lü, “Regular black holes from analytic $f(F^2)$,” *Eur. Phys. J. C* **83**, 755 (2023). doi:10.1140/epjc/s10052-023-11908-x arXiv:2303.16924 [gr-qc]
- [16] R.-Q. Yang, R.-G. Cai, and L. Li, “Constraining the number of horizons with energy conditions,” *Class. Quant. Grav.* **39**, 035005 (2022). doi:10.1088/1361-6382/ac3b41 arXiv:2104.03012 [gr-qc]
- [17] E. Poisson and W. Israel, “Internal structure of black holes,” *Phys. Rev. D* **41**, 1796–1809 (1990). doi:10.1103/PhysRevD.41.1796
- [18] R. Penrose, “Gravitational collapse: the role of general relativity,” *Riv. Nuovo Cim.* **1**, 252–276 (1969).
- [19] J. Sorce and R. M. Wald, “Gedanken experiments to destroy a black hole II: Kerr-Newman black holes cannot be overcharged or overspun,” *Phys. Rev. D* **96**, 104014 (2017). doi:10.1103/PhysRevD.96.104014 arXiv:1707.05862 [gr-qc]
- [20] C. W. Misner and D. H. Sharp, “Relativistic equations for adiabatic, spherically symmetric gravitational collapse,” *Phys. Rev.* **136**, B571–B576 (1964). doi:10.1103/PhysRev.136.B571
- [21] K. A. Bronnikov, “Regular magnetic black holes and monopoles from nonlinear electrodynamics,” *Phys. Rev. D* **63**, 044005 (2001). doi:10.1103/PhysRevD.63.044005 arXiv:gr-qc/0006014